564185

NUMERICAL SIMULATIONS OF ACOUSTICALLY DRIVEN, BURNING DROPLETS

H.-C. Kim, A. R. Karagozian, and O. I. Smith
Department of Mechanical and Aerospace Engineering
University of California, Los Angeles
Los Angeles, CA 90095-1597

Corresponding Author:

Professor A. R. Karagozian
Department of Mechanical and Aerospace Engineering
46-147D Engineering IV, UCLA
Los Angeles, CA 90095-1597
Phone: (310) 825-5653; FAX: (310) 206-4830
E-mail: ark@seas.ucla.edu

Paper 99F-50
Western States Section/The Combustion Institute
Fall Meeting, October, 1999

NUMERICAL SIMULATIONS OF ACOUSTICALLY DRIVEN, BURNING DROPLETS

H.-C. Kim, A. R. Karagozian, and O. I. Smith
Department of Mechanical and Aerospace Engineering
University of California, Los Angeles
Los Angeles, CA 90095-1597

1 Abstract

This computational study focuses on understanding and quantifying the effects of external acoustical perturbations on droplet combustion. A one-dimensional, axisymmetric representation of the essential diffusion and reaction processes occuring in the vicinity of the droplet stagnation point is used here in order to isolate the effects of the imposed acoustic disturbance. The simulation is performed using a third order accurate, essentially-non-oscillatory (ENO) numerical scheme with a full methanol-air reaction mechanism. Consistent with recent microgravity and normal gravity combustion experiments, focus is placed on conditions where the droplet is situated at a velocity antinode in order for the droplet to experience the greatest effects of fluid mechanical straining of flame structures. The effects of imposed sound pressure level and frequency are explored here, and conditions leading to maximum burning rates are identified.

2 Introduction

This study is part of a larger research program designed to understand and quantify the effects of pressure oscillations on the combustion characteristics of condensed fuels under microgravity conditions [1]. The issue of microgravity acoustic excitation of flames is especially pertinent to understanding the behavior of accidental fires which could occur in spacecraft crew quarters. The microgravity diffusion flames which could form are known to be very strongly affected by even small convective contributions[2]. Such disturbances could also be introduced by pressure perturbations within the crew quarters, e.g., as results from ventilation fans or engine vibrations. In normal gravity, studies have shown that there can be a significant increase in fundamental transport processes from reactive interfaces and surfaces with the imposition of an external acoustical field[3–7]. Under reduced gravity, natural convection is no longer a dominant process, and the effect of acoustics is likely to be far more pronounced.

2.1 Background

A comprehensive review of microgravity droplet combustion research through the early 1990s may be found in Law and Faeth[8]. A number of studies of droplet combustion in a microgravity environment indicate that the classical "d^2 law" [9] does describe the behavior of the droplet diameter, but that flame radius may not follow the law until a significant amount of time and droplet size reduction has elapsed[10, 11]. This observation is confirmed by experiments conducted in normal gravity but at very low pressures for small droplets[12] and is found to be associated with lower concentrations of fuel vapor adjacent to the flame at ignition than during later periods

of combustion when greater fuel vapor accumulation has occurred. A variety of fuels have been found to exhibit these characteristics [13, 14].

In a gravitational field, experiments have shown that there can be a significant increase in fundamental heat and mass transfer rates from reactive surfaces with the imposition of an external acoustical field[3–7]. The experiments of Blaszczyk[5] examined the effect of a stationary acoustic wave imposed on a single burning droplet. Blaszczyk measured up to a 14% increase in the combustion rate constant with acoustic excitation (compared with no acoustic excitation) in the excitation frequency range of 120-300 Hz and sound pressure level (SPL) range 100-115 dB. The experiments of Saito, et al.[4] also studied the effects of acoustic waves on single evaporating and burning fuel droplets, but with an examination of the effect of the position of the droplet, which was situated at either a pressure node or antinode. They found that when the fuel droplet was situated at a pressure node (velocity antinode), there was a two to three-fold increase in evaporative or combustion rate constants, but when the droplet was located at a pressure antinode (velocity node), there was little appreciable change in the evaporation or combustion rates.

To our knowledge, the only prior study which has involved acoustical excitation for burning droplets in microgravity is the very recent work by Tanabe, et al.[15, 16]. This experimental study involved the examination of burning droplets situated in an open duct, with imposed mean flow, and with a loudspeaker situated just outside of the duct to impose acoustic forcing. Fan-generated velocities were of the order 20 cm/sec, with acoustic forcing at frequencies ranging from about 50 hz to above 900 hz and sound pressure levels up to 140 dB. At an SPL of 125 dB, for example, the authors record velocities "in the vicinity of the droplet" which oscillate with an amplitude of ± 10 cm/sec, although it is not clear that a standing acoustic wave can be obtained in their duct at all flow conditions examined. These researchers observe significant increases in the burning rate constant as SPL is increased, especially when SPL increases from 125 dB to 135 dB, where a 50% increase in burning rate occurs. They also observe peaks in the droplet burning rate at acoustic frequencies near 400 hz and near 900 hz. These observations are consistent with corresponding normal gravity experiments by this group, although under microgravity conditions the increases in burning rate with increasing SPL are more dramatic than in normal gravity.

2.2 Present Study

In the present configuration, the droplet and surrounding diffusion flame are to be situated within an essentially one-dimensional (actually cylindrical) acoustic waveguide where standing waves are generated by a loudspeaker(s) placed at the end(s) of the guide, generating acoustic perturbations with varying frequency and amplitude. This configuration is shown schematically in Figure 1. For a waveguide length of 1 m, standing waves may be generated at frequencies above 200 hz, for example. Applied sound pressure levels in the experiments may be limited to magnitudes for which the droplet shape remains roughly spherical. In the present computations, however, larger sound pressure levels will be explored in order to be able to make at least qualitative comparisons with the trends seen in the microgravity experiments of Tanabe, et al.[15, 16].

The present computational study focuses on the essential changes in droplet burning rate that can occur when the droplet is exposed to acoustic excitation. A fully 3D or at least 2D axisymmetric representation of the droplet and flame, accounting for droplet and flame deformation, should be able to quantify precisely how such flame stretch results in augmented transport processes during acoustic excitation. But even a one-dimensional, axisymmetric representation of the essential

diffusion and reaction processes occuring in the vicinity of the droplet stagnation point can serve to quantify the effects of the acoustics (and associated acoustic time scales) on the reaction processes (with associated reaction, diffusion, and strain field time scales).

Hence as a preliminary study, the present paper describes the effects of perturbations in freestream velocity as experienced in the stagnation region of a methanol fuel droplet (methanol is one fuel expected to be examined in upcoming microgravity experiments [1]). In order to make at least some qualitative comparisons with the microgravity combustion experiments of Tanabe, et al.[15, 16], a mean flow $U_{\infty 1}$ is imposed on the droplet so as to always maintain a positive incoming velocity toward the drop surface, with or without acoustic excitation. Figure 2 shows a schematic diagram of the flow and boundary conditions in the vicinity of the droplet stagnation point. The "driving" velocity U_∞ is considered to be oscillatory in time, with an amplitude representative of conditions at a velocity antinode:

$$U_\infty = U_{\infty 1} + U_{\infty 2} sin\omega t \tag{1}$$

$U_{\infty 2}$ in fact can depend on the location at which the "freestream" driver is imposed in the computation, if the imposed frequencies are high enough (or wavelengths of excitation are small enough) to effectively reduce the perturbation velocity near the droplet.

Many studies of flames in the stagnation region of a blunt object or flame consider the driving flow to correspond to Hiemenz stagnation point flow [17–19], although in reality this is precisely accurate for large Reynolds numbers (based on droplet diameter). In the present case, however, the velocity perturbations do not create such large Reynolds numbers. For an applied SPL of 140 dB, for example, the maximum incoming velocity perturbations produce peak Reynolds numbers of the order 50; if the SPL is reduced to 120 dB, the Reynolds number is of the order 5. Thus in order to be more consistent with the magnitudes of imposed oscillatory velocities that are experienced by the burning droplets, the Oseen solution [17] for low Reynolds number flow about a spherical object is used as the farfield "driver" for the flow in the vicinity of the stagnation point, where $\theta \to 0$.

3 Problem Description and Methodology

The flow and reaction processes in the vicinity of the droplet are solved according to governing equations for species and energy conservation in an axisymmetric stagnation region with a low Mach number simplification [20]:

$$\vec{U}_t + \frac{1}{r^2}\left[r^2 \vec{G}(\vec{U})\right]_r = +\frac{1}{r^2}\left[r^2 \vec{G}_v(\vec{U})\right]_r + \vec{S} + \vec{C} \tag{2}$$

where

$$\vec{U} = \begin{pmatrix} e \\ \rho Y_1 \\ \rho Y_2 \\ \vdots \\ \rho Y_{NS} \end{pmatrix} \quad \vec{G}(\vec{U}) = \begin{pmatrix} (e+p)v_r \\ \rho v_r Y_1 \\ \rho v_r Y_2 \\ \vdots \\ \rho v_r Y_{NS} \end{pmatrix} \quad \vec{G}_v(\vec{U}) = \begin{pmatrix} Q_r \\ \rho D_{1m}(Y_1)_r \\ \rho D_{2m}(Y_2)_r \\ \vdots \\ \rho D_{NS,m}(Y_{NS})_r \end{pmatrix} \tag{3}$$

and

$$\vec{S} = \begin{pmatrix} 0 \\ \dot{\omega}_1 \\ \dot{\omega}_2 \\ \vdots \\ \dot{\omega}_{NS} \end{pmatrix} \qquad \vec{C} = \begin{pmatrix} -\epsilon(e+p) \\ -\epsilon\rho Y_1 \\ -\epsilon\rho Y_2 \\ \vdots \\ -\epsilon\rho Y_{NS} \end{pmatrix} \tag{4}$$

where the heat flux component, neglecting radiative heat transfer, is given by:

$$Q_r = \lambda T_r + \rho \sum_{k=1}^{NS} h_k D_{km} (Y_k)_r \tag{5}$$

The imposed "strain rate" ϵ is computed from Oseen flow to be, in the case of temporally varying inflow U_∞, dependent on both the spatial variable r and time t:

$$\epsilon\,(r,t) = \frac{U_\infty}{2r}\left[\left(\frac{r_o}{r}\right)^3 + 3\left(\frac{r_o}{r}\right) - 4\right] \tag{6}$$

where r is measured from the center of the droplet and the droplet radius r_o is assumed fixed at present, consistent with a computational reference frame that lies at the droplet surface.

Mass production rate terms $\dot{\omega}_i$ are evaluated in (4) in standard fashion, assuming an Arrhenius-type reaction rate coefficient dependence on temperature. In these computations all physical properties of the various species are assumed to be functions of temperature and are obtained using a transport package within CHEMKIN II[21]. Formulation of the ratio of specific heats for the mixture of gases present in a given computational cell is done so as to avoid thermodynamic inconsistencies in the presence of contact discontinuities, as described in Selerland and Karagozian [22]. A full kinetic mechanism for the combustion of methanol [23] is used in the present simulations. Finally, at the droplet surface in the present simulations, the Antoine relation is used to represent equilibrium evaporation.

The method of operator splitting via fractional steps, after Yamenko (e.g., as described in [24]), is employed to solve the system of equations (2). This procedure enables the system to be split into two separate equations, one which only includes the advection-diffusion terms and one which only includes the reaction rate source terms. The present method uses a third order essentially-non-oscillatory (ENO) [25] spatial integration to solve the advection-diffusion equation. ENO methods constitute a class of high accuracy, front capturing numerical schemes for hyperbolic systems of conservation laws, based on upwind biased differencing in local characteristic fields. The present scheme then employs a stiff ODE solver (VODE[26], an improved version of LSODE[27]) accompanied by the CHEMKIN-II package[21] to solve the temporally evolving equations with stiff source terms.

The present numerical methodology was validated by computing the steady state combustion behavior of a spherical methanol droplet in stagnant air and comparing results with the numerical simulations of Marchese, et al [23]. As shown in Figures 3ab, the distributions of methanol fuel, oxygen, products, OH radical, and temperature appear to compare reasonably well with these prior computations, which used the same chemical mechanism but with a different numerical scheme for the axisymmetric droplet. Comparisons are especially accurate in the vicinity of the droplet surface and on the "fuel" side of the diffusion flame. Because the present scheme is designed to be able to accomodate acoustic time scales, the farfield steady state condition takes much longer (in

computational time) to reach in the present computation, and hence there are some discrepancies between the present simulations and the steady state simulations of Marchese, et al [23] far from the droplet surface. Nevertheless, the essential features of the present model (transport processes near the stagnation point) appear to be the same as in these prior studies.

4 Results

The present computations were carried out for several different amplitudes and frequencies of acoustic excitation of the droplet. In all conditions it is assumed that the droplet is situated at the velocity antinode of a standing wave in order to produce the maximum effect on burning, as seen by Saito, et al. [4]. Hence temporal and spatial pressure variation here is minimal. There is also a mean flow $U_{\infty 1}$ imposed in the flowfield, consistent with the experiments of Tanabe, et al. [15, 16], so that there is continuous positive inflow to the droplet stagnation point.

The computational domain in this problem extends from the droplet surface (with effective droplet radius r_o = 1 mm) to a distance 2 cm into the flowfield. In most computations shown here the mean velocity $U_{\infty 1}$ is of the order 22 cm/sec with a sound pressure level of 140 dB, which results in a velocity amplitude $U_{\infty 2}$ of 22 cm/sec. In a few cases, both "unforced" flow (in which $U_{\infty 1} = U_{\infty 2} = 0$) and flow that is "forced without oscillation" (i.e., $U_{\infty 2} = 0$) will also be examined. As noted previously, the perturbation velocity actually can be reduced at high frequencies for a fixed computational domain, since at frequencies above several hundred hertz, the effective freestream velocity seen by the droplet will be reduced from its velocity peak within the waveguide. This variation in U_∞ will be explored in these computations.

Average fuel mass flux at the droplet surface (temporally averaged over one period) as a function of time is shown in Figures 4 and 5, for the cases where $U_{\infty 1}$ and $U_{\infty 2}$ are both independent and dependent, respectively, on the frequency imposed within the waveguide. Quasi-steady burning appears to be reached at about 0.12 sec after ignition in both cases. In the case where the freestream velocity components are independent of frequency, as in Figure 4, the quasi-steady burning rate increases with frequency, but appears to asymptote to the same values for frequencies above 1000 hz. For the case where the freestream velocity components can be reduced at the edge of the computational domain at high frequencies, as in Figure 5, the quasi-steady burning rate increases with frequency until about 200-400 hz, then the burning rate decreases with frequency above 400 hz. Figure 6 displays more clearly the quasi-steady burning rate (at times exceeding 0.15 sec) as a function of imposed frequency for this condition. These observations are in fact consistent with the observations of Blaszczyk [5] in normal gravity, and with Tanabe, et al. [15, 16] in microgravity experiments, who both observed peaks in the droplet burning rate at acoustic frequencies near 200-400 hz despite the fact that they used different fuels. The fact that the present computations produce peaks at nearly the same acoustic conditions suggests that the peaks may be due to the reduction in the effective freestream velocity amplitude seen by the droplet at higher frequencies. The present simulations also show a monotonic decrease in burning rate as the imposed frequency increases above 400 hz, consistent with the observations of Blaszczyk [5], but in contrast to the second increase in burning rate seen by Tanabe, et al. [15, 16] at frequencies above 900 hz. This second increase may be due to acoustic resonances which are specific to the open duct geometry used in these microgravity experiments [15, 16] which is not represented in the present computational studies and also not used in the normal gravity experiments of Blaszczyk [5].

The instantaneous mass flux at the droplet surface as a function of time (portion of an acoustic

cycle) for different imposed frequencies is shown in Figure 7a; Figure 7b shows the temporally varying freestream velocity U_∞ which is imposed for a SPL of 140 dB. Figure 7a represents the case where the amplitude of oscillation is considered constant or independent of the computational domain. These results show that the excursions in mass blowing/burning rate at the surface are large at lower frequencies and diminish at higher frequencies. The mean mass flux for the lower frequencies, however, appears to be lower than that for higher frequencies. At higher frequencies in fact the mean mass flux at the droplet surface appears to be close to that for the case where the incoming velocity is non-oscillatory, i.e., $U_{\infty 2} = 0$. This observation is consistent with diffusion as well as premixed flame studies that examine the exposure of the flame to an oscillatory strain field [22, 28]. At very high frequencies, the flame often has difficulty keeping up with the oscillations (some of the reactions have characteristic times that become close to the order of the acoustic time) and effectively begins to behave like a flame exposed to a constant rate of strain. It is interesting to note that there appears to be a phase shift between the temporal mass blowing rate in Figure 7a and the imposed oscillatory velocity field in Figure 7b; this phase shift increases with higher imposed frequencies of oscillation.

These trends in instantaneous burning rate may also be explained by examining the variation in flame (maximum) temperature as a function of the acoustic cycle, as well as the variable position of the flame in time, as shown in Figures 8ab. As seen in Figure 8a, the excursions in magnitude of the (peak) flame temperature are much greater for lower frequencies, where the oscillations in peak temperature at very high frequency are very small and close to the steady state temperature computed for a constant inflow condition ($U_{\infty 2} = 0$). In many of the lower frequency cases, the mean flame temperature also appears to be slightly lower than for the steady state case, but this is not an entirely consistent trend. The position of the flame shown in Figure 8b explains some of these features. At lower frequencies of excitation, the flame periodically moves very close to the droplet surface, closer than is achieved at higher frequencies, upon which the mass flow rate peaks as seen in Figure 7a. Although the flame temperature itself appears to be at a temporal minimum when the flame moves close to the droplet surface, it nevertheless heats the droplet to the extent that the evaporative blowing rate increases. The almost indiscernible motion of the flame at very high frequencies of excitation (1000 hz and above) confirms that the flame is unable to respond to any significant degree to the imposed acoustic field at such conditions.

Finally, Figure 9 shows the time-averaged fuel mass flux at the droplet surface when the frequency of the oscillation is fixed at 200 hz but where the amplitude of acoustic oscillation is altered such that SPLs vary from 110 dB to 140 dB. These results show that the increases in burning rate are not very pronounced as one increases the SPL from 110 to 120 dB, but as one goes from 120 to 130 to 140 dB (where corresponding velocity perturbations are much higher, according to the logarithmic dB scale used for SPL), a significant (25%) increase in burning rate occurs. It appears that these large increases in velocity perturbation (at a velocity antinode) can lead to especially large increases in the oscillatory rates of strain experienced by diffusion flames bounding the droplet, leading to large increases in the droplet burning rate. These observations are consistent with the experimental observations of Tanabe, et al. [15, 16] in microgravity, although the experiments suggested that even higher burning rate augmentation levels are possible.

5 Conclusions

This computational study has focused on understanding and quantifying the effects of external acoustical perturbations on droplet combustion. A one-dimensional, axisymmetric representation of the essential diffusion and reaction processes occuring in the vicinity of the droplet stagnation point is used here in order to isolate the effects of the imposed acoustic disturbance. Thus while the present model clearly does not capture all complexities in this acoustically driven, reactive flowfield, it does represent the essential phenomena to the extent that results are consistent with experimental observations. With increasing imposed frequencies, an increase in the average droplet burning rate is observed until a finite range (200-400 hz), after which the burning rate decreases. This phenomenon appears to be associated with the effective reduction in the perturbation velocity "seen" by the droplet at higher frequencies, and is quantitatively similar to experimental observations in normal gravity [5] as well as microgravity [15, 16]. Burning rate is also seen to increase significantly when one increases the SPL from 130 to 140 dB, which produces large increases in the oscillatory strain rate of the flow, again consistent with experimental observations [15, 16].

Clearly, interactions among chemical, diffusion, acoustic, strain field time scales control the phenomena observed in this problem. When acoustic time scales are relatively small (at very high imposed frequencies), they approach the order of magnitude of some of the chemical times associated with combustion reactions, and the reaction itself has difficulty keeping up with the imposed high frequency oscillation. At lower imposed frequencies (higher acoustic times), the reaction becomes comparatively "fast", allowing the diffusion-limited flame structure to be perturbed more strongly by the imposed acoustic field.

While future work in this study will include more complex droplet and flame geometries for the acoustically driven, burning droplet, it is useful to know that the esstential features of the transport phenomena can be extracted from a relatively simple one-dimensional formulation of the problem.

6 Acknowledgements

The authors wish to thank Professor Fred Dryer of Princeton University, who kindly provided CHEMKIN input data for the methanol kinetic mechanism used in this study. This study is being supported by the NASA Microgravity Combustion Program under Grant NCC3-690, with Drs. Ming-Shin Wu and Kurt Sacksteder as grant monitors.

7 References

References

[1] Smith, O. I., Karagozian, A. R., Kim, H.-C., and Ghenai, C., "Acoustically Forced, Condensed Phase Fuel Combustion under Microgravity Conditions" Proc. of the Fifth International Microgravity Combustion Workshop, pp 469-472, May 18-20, 1999.

[2] Friedman, R. and Urban, D., *NASA TM-101397*, 1989.

[3] Marthelli, R. C. and Boelter, L. M. K., *Proc. 5th Int. Congress of Applied Mechanics*, 578-584, 1939.

[4] Saito, M., Sato, M., and Suzuki, I., *Fuel, 73*, 349-353, 1994.

[5] Blaszczyk, J., *Fuel, 70*, 1023-1025, 1991.

[6] Zinn, B. T., Carvalho, J. A., Jr., Miller, N., and Daniel, B. R., *19th Symp. (Intl.) on Comb.*, 1197, 1982.

[7] Rudinger, G., *J. Fluids Engr.*, 321-326, 1975.

[8] Law, C. K. and Faeth, G. M., *Prog. Energy Combust. Sci., 20*, 65-113, 1994.

[9] Law, C. K., *Prog. Energy Combust. Sci., 8*, 171, 1982.

[10] Kumagai, S., Sakai, T., and Okajima, S., *13th Symp. (Intl.) on Comb.*, 779-785, 1970.

[11] Hara, H. and Kumagai, S., *23rd Symp. (Intl.) on Comb.*, 1605-1610, 1990.

[12] Law, C. K., Chung, S. H., and Srinivasan, N., *Combust. Flame, 38*, 173, 1980.

[13] Choi, M.Y., Dryer, F. L., and Haggard, J. B., Jr., *23rd Symp. (Intl.) on Comb.*, 1597-1604, 1990.

[14] Shaw, B. D., Dryer, F. L., Williams. F. A., and Haggard, J. B., *Acta Astronautica, 17*, 1195, 1988.

[15] Tanabe, M., Aoki, K., Sato, K., and Fujimori, T., "Influence of Acoustic Field on Droplet Burning in Microgravity", Proc. of the Fifth International Microgravity Combustion Workshop, NASA Lewis Research Center, May 18-20, 1999, pp. 249-252.

[16] Tanabe, M., Morita, T., Aoki, K., Sato, K., and Fujimori, T., "Evaluation of the Influences of Acoustic Field on Droplet Burning using Microgravity", talk presented at the International Seminar on Microgravity Combustion, Tohoku University, August 19-20, 1999.

[17] Panton, R., **Incompressible Flow**, Wiley-Interscience, 1984.

[18] Tsuji, H. and Yamaoka, I., *19th Symp. (Intl.) on Comb.*, 1533, 1982.

[19] Darabiha, N. and Candel, S., *Combust. Sci. Tech.* 86: 67-85 (1992).

[20] Majda A. and Sethian, J., *Combust. Sci. Tech.* 42, p. 185 (1985).

[21] Kee, R. J., Miller, J. A., and Jefferson, T. H. (1980). CHEMKIN: A general purpose, problem independent, transportable, Fortran chemical kinetics code package. Sandia National Laboratories Report SAND80-8003.

[22] T. Selerland and A. R. Karagozian, *Comb. Sci. Tech., 131*, No. 1-6, pp. 251-276 (1998).

[23] Marchese, A.J., Nayagam, N.V., Colantonio, R., and Dryer, F.L., *26th Symp. (Int.) on Comb.*, 1209, 1997.

[24] Strikwerda, J. C., **Finite Difference Schemes and Partial Differential Equations**, Wadsworth and Brooks, 1989.

[25] Shu, C.W., Osher, S., *J. Comput. Phys.*, Vol. 83, pp. 32-78, 1989.

[26] Brown, P. N., Byrne, G. D., and Hindmarsh, A. C., *SIAM J. Scientific Statistical Computing* 10, pp. 1038-1051, 1989.

[27] Hindmarsh, A. C., *Scientific Computing*, R. S. Stepleman, *et al.*, eds., North-Holland, Amsterdam, pp. 55-64, 1983.

[28] Egolfopoulos, F. N., *Twenty-fifth Symposium (International) on Combustion*, The Combustion Institute, Pittsburgh, PA, pp. 1365-1373, 1994.

8 Nomenclature

NS number of species
Q_r r-component of heat flux vector
T temperature
Y_i mass fraction of species i
e energy of the mixture per unit volume
h_i enthalpy per unit volume of species i
p pressure
r radial coordinate measured from the center of the droplet
r_o droplet radius
t time
U_∞ "farfield" velocity approaching the droplet surface $= U_{\infty 1} + U_{\infty 2} sin\omega t$
v_r local gas velocity in the r-direction

ϵ effective strain rate imposed by farfield Oseen flow
λ thermal conductivity of the mixture
ρ mixture density
ω frequency of imposed acoustic oscillation
$\dot{\omega}_i$ mass production rate of species i

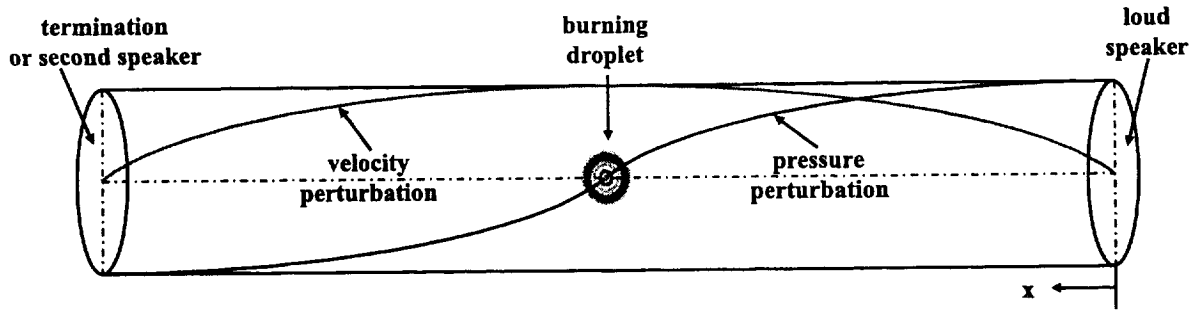

Figure 1: Schematic diagram of a fuel droplet situated at a pressure node (velocity antinode) within an acoustic waveguide.

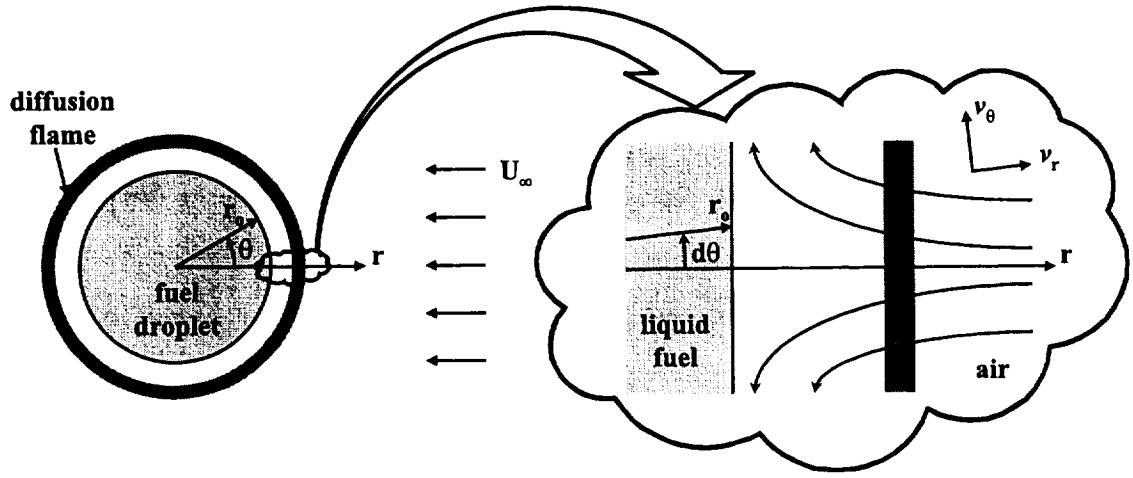

Figure 2: Schematic diagram of freestream flow over a fuel droplet and the flow within the stagnation region of a burning droplet.

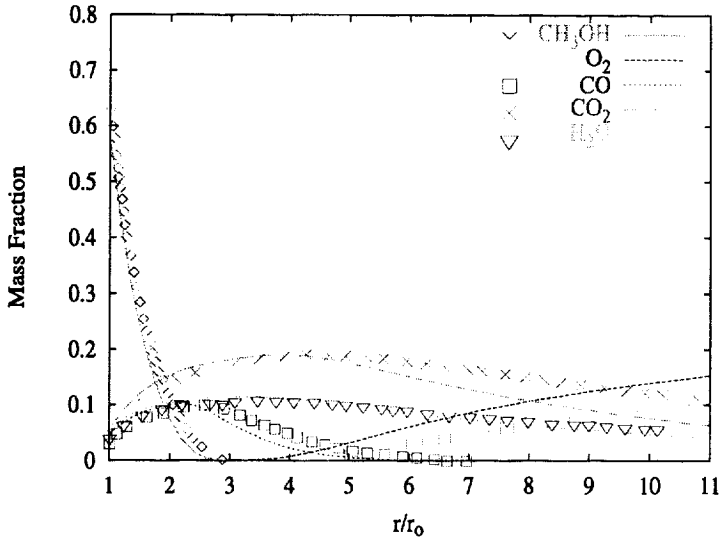

(a)

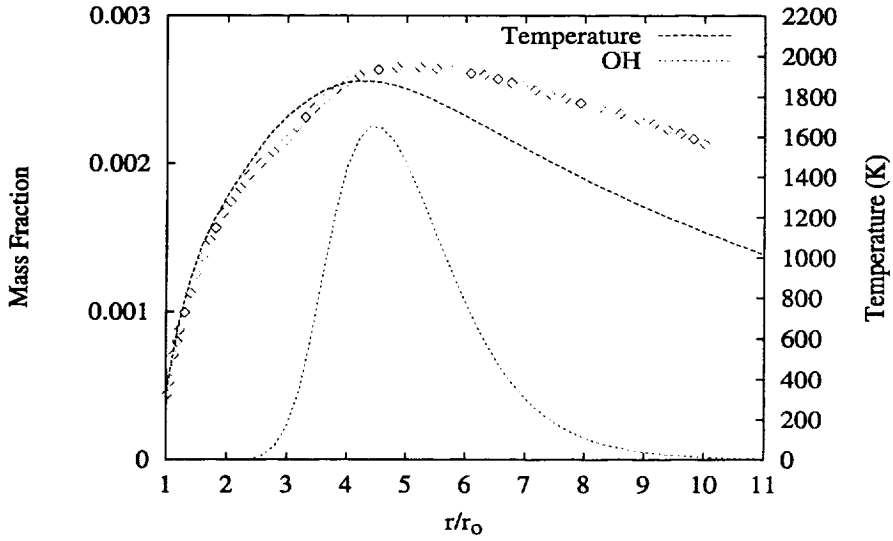

(b)

Figure 3: Results from the present computational method for steady state species and temperature distributions measured from the surface of a spherical methanol droplet burning in quiescent air. Comparisons are made with the simulations of Marchese, et al [23].

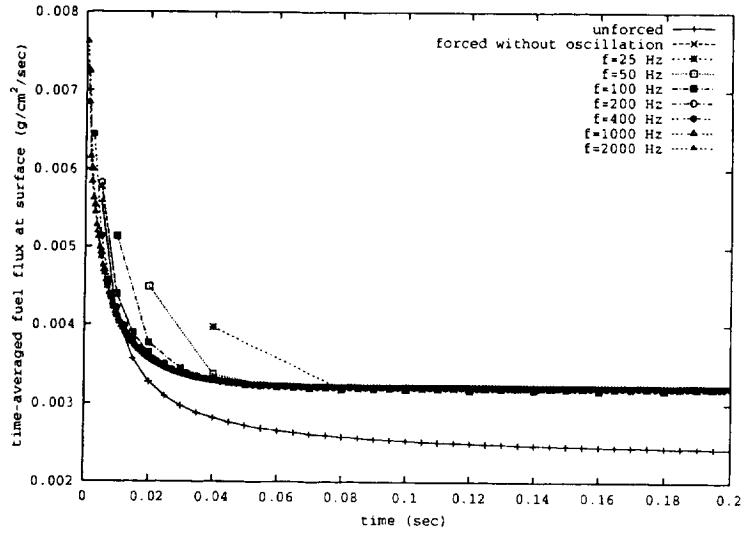

(a)

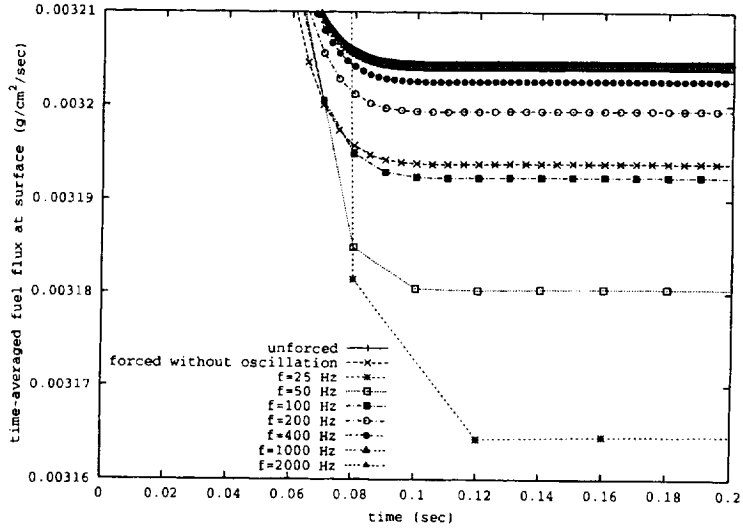

(b)

Figure 4: Results from the present computational method for the mass flux at the droplet surface (burning rate), averaged in time over an acoustic cycle, as a function of time for different imposed frequencies. Part (b) displays the results on an expanded scale. Here the freestream velocity perturbation is assumed to be constant, i.e., independent of frequency. The imposed velocity perturbation corresponds to a sound pressure level SPL of 140 dB, with a mean incoming velocity of 22 cm/sec.

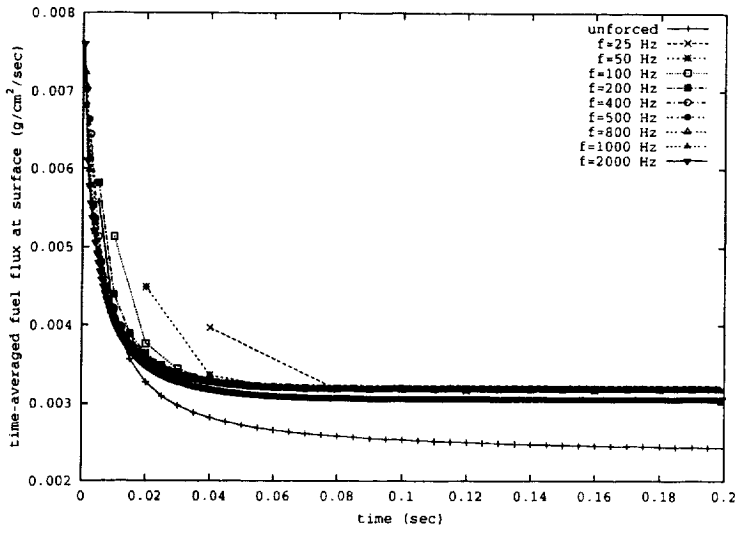

(a)

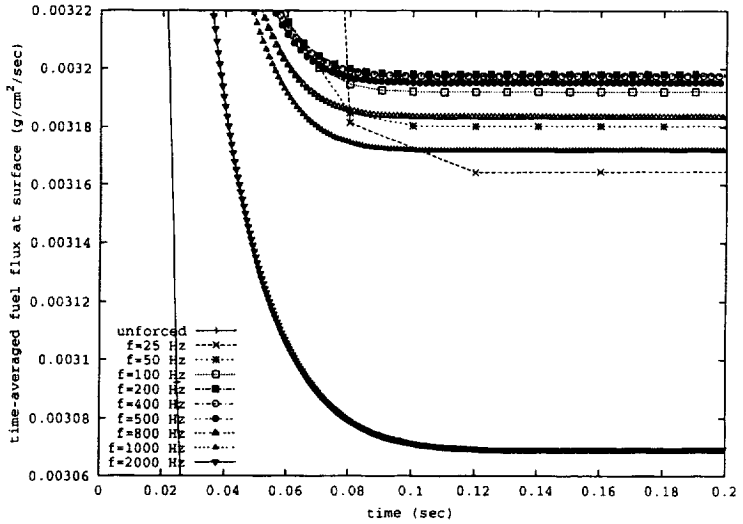

(b)

Figure 5: Results from the present computational method for the mass flux at the droplet surface (burning rate), averaged in time over an acoustic cycle, as a function of time for different imposed frequencies. Part (b) displays the results on an expanded scale. Here the freestream velocity perturbation is assumed to be reduced at the edge of the computational domain when required by a high frequency within the waveguide. The imposed velocity perturbation corresponds to a sound pressure level SPL of 140 dB, with a mean incoming velocity of 22 cm/sec.

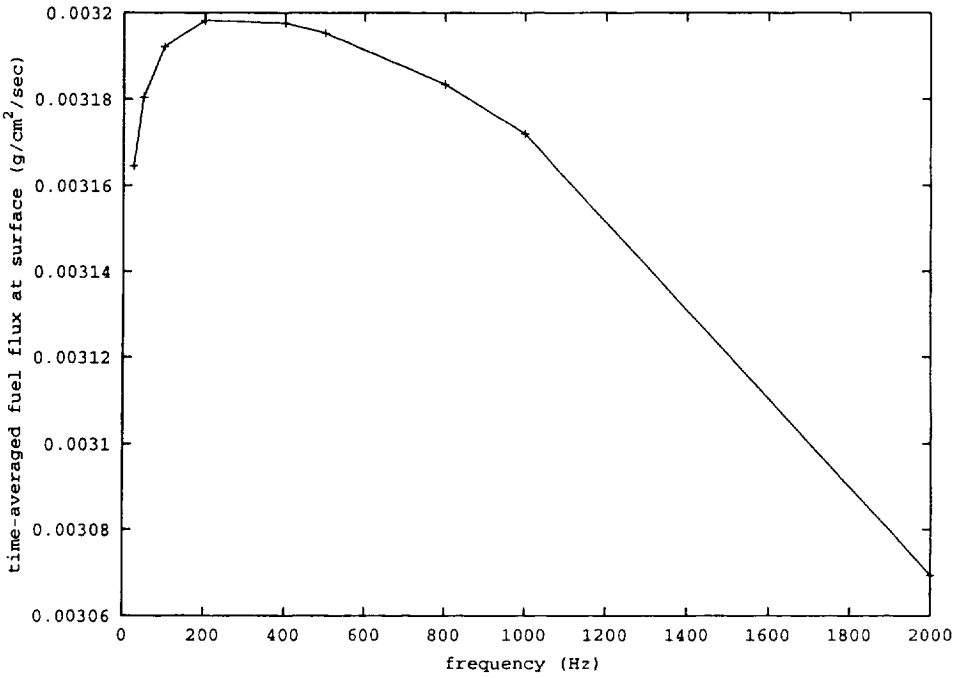

Figure 6: Results from the present computational method for the mass flux at the droplet surface (burning rate), averaged in time over an acoustic cycle, as a function of imposed frequency. Here the freestream velocity perturbation is assumed to be reduced at the edge of the computational domain when required by a high frequency within the waveguide. The imposed velocity perturbation corresponds to a sound pressure level SPL of 140 dB, with a mean incoming velocity of 22 cm/sec.

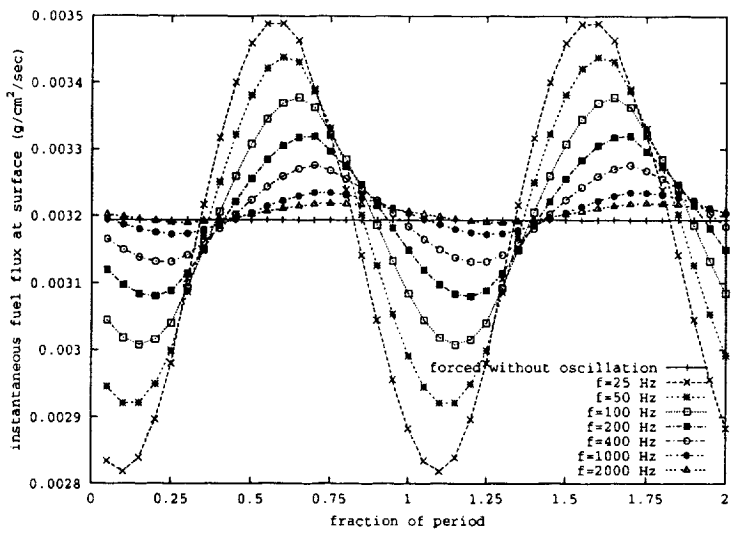

(a) instantaneous $\dot{m}_f$

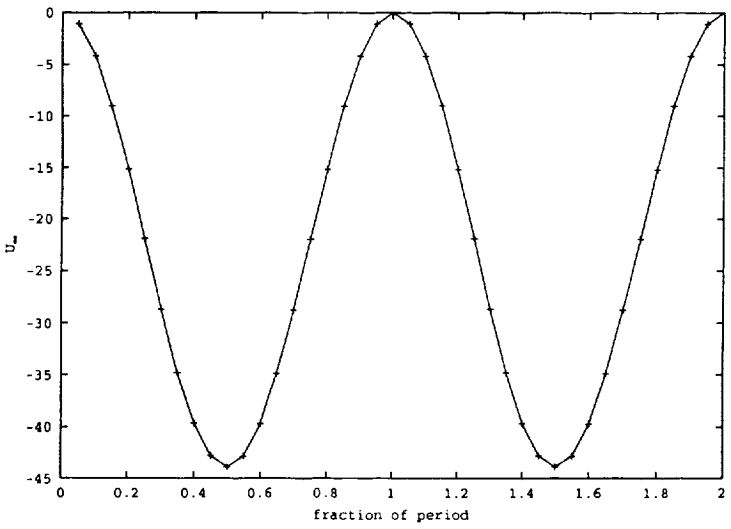

(b) imposed freestream velocity

Figure 7: (a) The instantaneous mass flux at the droplet surface (burning rate) as a function of the fraction of the acoustic period for different imposed frequencies. (b) The imposed velocity perturbation at the edge of the computational domain corresponding to a sound pressure level SPL of 140 dB, with a mean incoming velocity of 22 cm/sec.

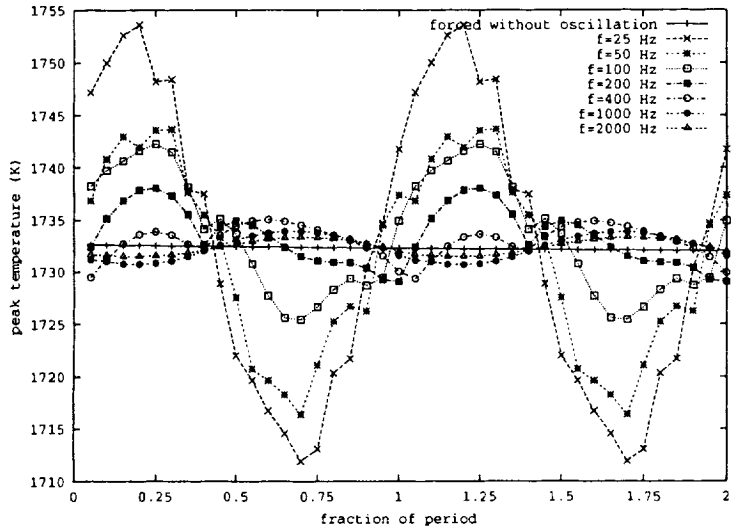

(a) instantaneous flame temperature

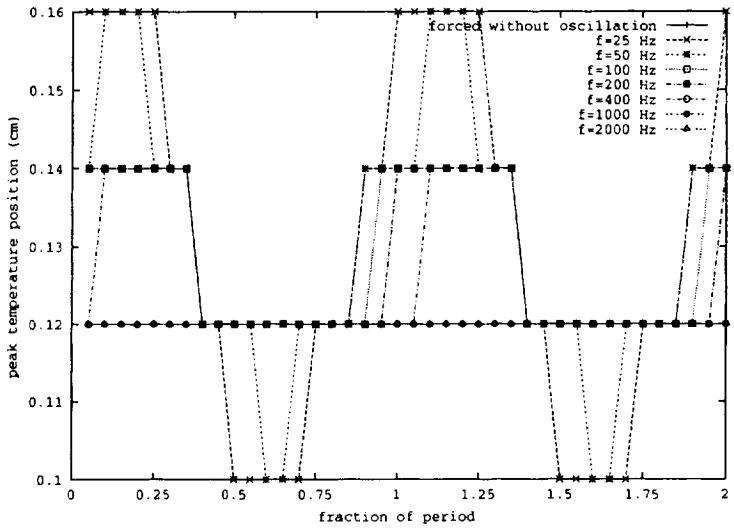

(b) instantaneous peak temperature location

Figure 8: (a) The instantaneous peak (flame) temperature in the flowfield as a function of the fraction of the acoustic period for different imposed frequencies. (b) The location of the peak (flame) temperature in the flowfield as a function of the fraction of the acoustic period for different imposed frequencies. The imposed velocity perturbation corresponds to a sound pressure level SPL of 140 dB, with a mean incoming velocity of 22 cm/sec.

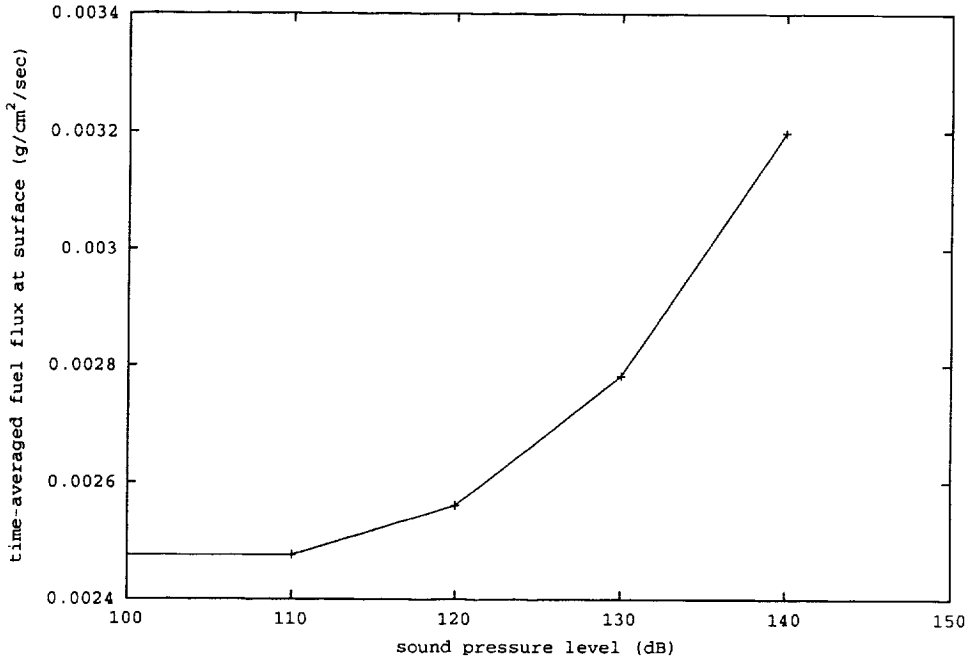

Figure 9: Results from the present computational method for the mass flux at the droplet surface (burning rate), averaged in time over an acoustic cycle, as a function of imposed sound pressure level SPL at a fixed frequency of 200 hz. Here the freestream velocity perturbation is assumed to be reduced at the edge of the computational domain when required by a high frequency within the waveguide.